Gap vortex solitons in periodic media with quadratic nonlinearity

Chao Hang,[1] Vladimir V. Konotop,[1,2] and Boris A. Malomed[3]
[1]*Centro de Física Teórica e Computacional, Universidade de Lisboa, Complexo Interdisciplinar, Avenida Professor Gama Pinto 2, Lisboa 1649-003, Portugal*
[2]*Departamento de Física, Faculdade de Ciências, Universidade de Lisboa, Campo Grande, Ed. C8, Piso 6, Lisboa 1749-016, Portugal*
[3]*Department of Physical Electronics, School of Electrical Engineering, Faculty of Engineering, Tel Aviv University, Tel Aviv 69978, Israel*

(Received 3 June 2009; published 27 August 2009)

We explore the existence and stability of two-dimensional spatial gap solitons with embedded vorticity in a bulk medium with the quadratic ($\chi^{(2)}$) nonlinearity and a transverse grating represented by periodic modulation of the refractive index. Gap-vortex solitons (GVSs) can be found in *total gaps* of the underlying spectra of the fundamental-frequency and second-harmonic waves. We demonstrate the existence of a family of stable GVSs, which are built as four-peak complexes, in the lowest total gap. We also consider dynamical effects, such as self-trapping of GVSs from input beams, and delocalization transitions.

DOI: 10.1103/PhysRevA.80.023824 PACS number(s): 42.65.Tg, 42.70.Qs, 42.65.Ky, 05.45.Yv

I. INTRODUCTION

Experimental and theoretical studies of spatial, temporal, and spatiotemporal solitons in optical media with various nonlinearities have grown into a tremendous field of research [1], starting from the prediction of famous (although unstable) Townes' solitons [2]. Two-dimensional (2D) and three-dimensional (3D) solitary vortices, i.e., solitons with embedded vorticity, have also been predicted in these settings [3]. In uniform bulk media with cubic, saturable, and quadratic nonlinearities, spatial ring-shaped vortex solitons are unstable against azimuthal perturbations (in addition to the instability against the collapse in the cubic medium), as forecast theoretically [4] and demonstrated experimentally [5]. However, vortices may be made stable in media featuring competing [cubic-quintic, $\chi^{(3)}:\chi^{(5)}$, or quadratic-cubic, $\chi^{(2)}:\chi^{(3)}$] nonlinearities [6] or effective lattice potentials induced by transverse *gratings* in the form of periodic modulation of the local refractive index. The latter mechanism was theoretically predicted [7–9] and demonstrated in experiments, using photoinduced lattices in photorefractive crystals, where the nonlinearity is saturable [10–12]. The combination of the cubic-quintic nonlinearity and grating-induced periodic potential was considered too [13].

The light propagation in nonlinear media with transverse gratings exhibits a variety of specific features originating from the grating-induced band-gap spectrum of the system. In particular, the mechanism behind the formation and stabilization of the above-mentioned solitary vortices is the interplay of the wave tunneling between adjacent cells of the periodic potential and local nonlinearity. It has been predicted that, in addition to the fundamental vortices, with topological charge $S=1$, this setting may also support stable higher-order vortices, with $S\geq 2$, and "supervortices" in the form of a ring-shaped chain of compact vortices with individual topological charges $s=1$, global vorticity $S=\pm 1$ being imprinted onto the chain [9]. The localized patterns with $S=2$ and quadrupoles [11], as well as chains built of fundamental vortices [12], have been created in the experiment. Generally, possible types of higher-order localized vortices are restricted by the symmetry of the underlying lattice potential [14]. Three-dimensional (spatiotemporal) vortex solitons supported by a low-dimensional 2D lattice have been predicted too [15] (stable 3D solitary vortices may also be stabilized by completing nonlinearities in uniform media [16]).

The subject of this work are 2D spatial vortex solitons in a medium carrying the $\chi^{(2)}$ (alias second-harmonic-generating) nonlinearity in the combination with the transverse grating. As usual, the $\chi^{(2)}$ solitons are composed of fundamental-frequency (FF) and second-harmonic (SH) components. The model is formulated in Sec. II. Examples of localized vortices in such a setting have been previously reported in Ref. [17], where, in particular, an existence border (cut-off value) was found for the propagation constant of vortex solitons. In this context, it is relevant to mention that a different type of *spatial-spectral* vortices can be supported in a discrete system [18], which may be considered as a counterpart of the continuous model considered in the present paper (the correspondence between the models can be obtained in the proper limit by means of the Wannier-function expansion [19]).

In Sec. III, which reports main results obtained in this work, we carry out the analysis of this physical model. First, we establish an intrinsic relation of the cutoff to the band-gap spectra induced by the underlying grating. The propagation constants of the FF and SH components of vortical modes do not necessarily fall into the semi-infinite gaps of the respective spectra (the situation reported in Ref. [17]), unless one deals with the case when no finite band gaps open in each component [20]. In the general situation, solitons exist for propagation constants (frequencies ω and 2ω, in terms of our notation) belonging to one of the *total gaps* of the FF and SH spectra, which means that both ω and 2ω must fall into respective gaps [similar to the one-dimensional (1D) situation considered in Ref. [21]]. Thus, we report the existence of the solitons belonging to finite band gaps of the FF and SH spectra. The phase-mismatch constant is an essential parameter controlling the existence domains—varying it, one can change the number of the total gaps. In this connection, it is relevant to mention that binary solitons with two components

belonging to different spectral gaps (in particular, one semi-infinite, and another one being the first or second finite band gap) were reported in the model of a Bose-Einstein mixture loaded into 1D or 2D lattice potentials [22]. We also explore dynamical effects, such as the generation of the SH component and the delocalization transition, which was first studied in detail in the 2D model combining the grating potential and cubic self-focusing nonlinearity [23] (for a brief review of the latter topic, see Ref. [24]).

II. MODEL

We start with the well-known coupled evolution equations for complex amplitudes α_1 and α_2 of the FF and SH fields in the spatial domain with coordinates $\mathbf{r}=(x,y)$ [25]:

$$i\frac{\partial\alpha_1}{\partial t}=-\frac{1}{2}\nabla^2\alpha_1+\varepsilon_1(\mathbf{r})\alpha_1-\bar{\alpha}_1\alpha_2, \tag{1a}$$

$$i\frac{\partial\alpha_2}{\partial t}=-\frac{1}{4}\nabla^2\alpha_2+\varepsilon_2(\mathbf{r})\alpha_2-\frac{1}{2}\alpha_1^2+q\alpha_2. \tag{1b}$$

Here evolution variable t stands for the propagation distance in the bulk quadratically nonlinear medium, with the respective $\chi^{(2)}$ coefficient scaled to be 1, the transverse diffraction is accounted for by $\nabla^2=\partial^2/\partial x^2+\partial^2/\partial y^2$, q is the phase-mismatch parameter, and the transverse grating is represented by the periodic functions, $\varepsilon_{1,2}(\mathbf{r})=\varepsilon_{1,2}(\mathbf{r}+\mathbf{a}_j)$, where $\mathbf{a}_{1,2}$ are the corresponding lattice vectors. The system can be written in the Hamiltonian form, $\partial\alpha_{1,2}/\partial t=-i\delta H/\delta\bar{\alpha}_{1,2}$, with Hamiltonian

$$H=\int\left[\frac{1}{2}|\nabla\alpha_1|^2+\frac{1}{4}|\nabla\alpha_2|^2+\varepsilon_1(\mathbf{r})|\alpha_1|^2+\varepsilon_2(\mathbf{r})|\alpha_2|^2-\frac{1}{2}\bar{\alpha}_1^2\alpha_2-\frac{1}{2}\alpha_1^2\bar{\alpha}_2+q|\alpha_2|^2\right]d\mathbf{r} \tag{2}$$

(the overbar stands for the complex conjugation). In addition to the Hamiltonian, another conserved quantity is the total power of the optical beam, alias the Manley-Rowe invariant, $P=\int(|\alpha_1|^2+2|\alpha_2|^2)d\mathbf{r}$.

We are interested in stationary solutions to Eqs. (1), $\alpha_m=\beta_m(\mathbf{r})\exp(-im\omega t)$ with $m=1,2$. The substitution of this into Eqs. (1) leads to the spatial equations,

$$-\nabla^2\beta_1+2\varepsilon_1(\mathbf{r})\beta_1-2\bar{\beta}_1\beta_2=2\omega\beta_1, \tag{3a}$$

$$-\frac{1}{4}\nabla^2\beta_2+\varepsilon_2(\mathbf{r})\beta_2-\frac{1}{2}\beta_1^2+q\beta_2=2\omega\beta_2. \tag{3b}$$

Soliton solutions of Eqs. (3) are intrinsically related to the corresponding Bloch modes, $\beta_{\nu,\mathbf{k}}^{(m)}(\mathbf{r})$, which are solutions of the respective linearized problems,

$$\mathcal{L}_m\beta_{\nu,\mathbf{k}}^{(m)}(\mathbf{r})=\mathcal{E}_{\nu,\mathbf{k}}^{(m)}\beta_{\nu,\mathbf{k}}^{(m)}(\mathbf{r}),m=1,2, \tag{4}$$

with $\mathcal{L}_m\equiv-(1/m^2)\nabla^2+(2/m)\varepsilon_1(\mathbf{r})$. Here, subscript $\nu=1,2,\ldots$ enumerates allowed Bloch bands, and $\mathbf{k}$ designates the wave vector in the first Brillouin zone. We consider the square lattice, with $\mathbf{a}_1\cdot\mathbf{a}_2=0$ and normalization

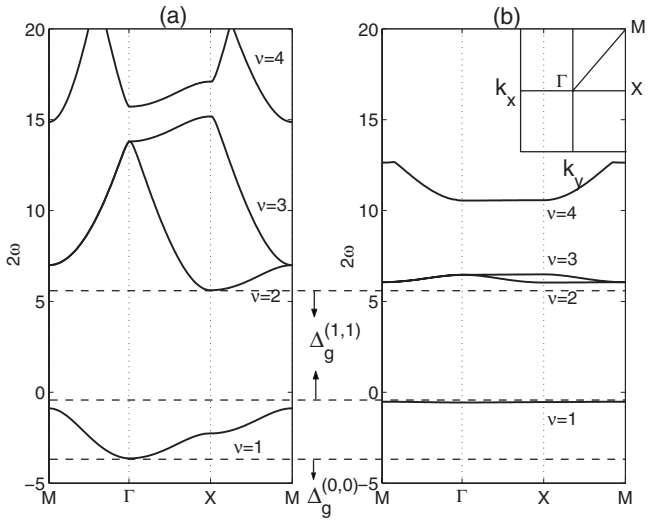

FIG. 1. The band-gap structures of the FF (a) and SH (b) components for grating (5). Shown are the four lowest bands, with $\nu=1,\ldots,4$. The phase mismatch is $q=-8.0$. In this case, the single total gap, whose limits are indicated by the horizontal dashed lines, is $\Delta_g^{(1,1)}\approx 6.0$. The inset in panel (b) shows the standard notation used for the high-symmetry points of the first Brillouin zone.

$|\mathbf{a}_1|=|\mathbf{a}_2|=\pi/2$, hence $\mathbf{k}\in[-2,2]\times[-2,2]$. We will also use notations $\mathcal{E}_{\nu,\pm}^{(m)}$ for the lower ("−") and upper ("+") edges of the νth band, and $\Delta_\nu^{(m)}\equiv\mathcal{E}_{\nu+1,-}^{(m)}-\mathcal{E}_{\nu,+}^{(m)}$ for the width of the gap separating the νth and $(\nu+1)$th bands. An example of the band-gap structures for the usual cosinusoidal grating (with strength ε_0),

$$\varepsilon_2(\mathbf{r})=2\varepsilon_1(\mathbf{r})=2\varepsilon_0[\cos(4x)+\cos(4y)], \tag{5}$$

is shown in Fig. 1.

Assuming that finite band gaps exist for both components, Eqs. (3) may give rise to exponentially localized solutions only if there is a nonzero overlap between the two band gaps, i.e., if there is a *total gap*, $\Delta_g^{(\nu,\nu')}\equiv\Delta_\nu^{(1)}\cap\Delta_{\nu'}^{(2)}\neq 0$ (for a more detail discussion of the required band-gap structure of the coupled $\chi^{(2)}$ system, see Ref. [21]). The existence of the total gap is always achievable by adjusting mismatch q, which determines the relative position of the band-gap structures in the SH and FF components, provided that a gap exists in each of them (the latter requirement is relevant to the 2D case, as in the 1D case a periodic potential always induces at least a finite number of gaps).

By analogy with the 1D case [21], one can establish that if a stationary localized solution (β_1,β_2) exists, it satisfies integral relations

$$\int[|\beta_1(\mathbf{r})|^2\nabla\varepsilon_1(\mathbf{r})+|\beta_2(\mathbf{r})|^2\nabla\varepsilon_2(\mathbf{r})]d\mathbf{r}=0,$$

$$\mathrm{Im}\left\{\int\bar{\beta}_1^2(\mathbf{r})\beta_2(\mathbf{r})d\mathbf{r}\right\}=0, \tag{6}$$

which represent necessary conditions for the existence of localized modes and thus impose constrains on admissible distributions of the intensity. Then, introducing

$$H_V(\mathbf{r}) = \int [\varepsilon_1(\mathbf{r}'+\mathbf{r})|\beta_1(\mathbf{r}')|^2 + \varepsilon_2(\mathbf{r}'+\mathbf{r})|\beta_2(\mathbf{r}')|^2]d\mathbf{r}', \tag{7}$$

the necessary existence conditions, given by Eq. (6), can be rewritten as $\nabla H_V(\mathbf{r})|_{\mathbf{r}=0}=0$, while necessary conditions for the stability of the solitons take the form of

$$\left[\frac{\partial^2 H_V(\mathbf{r})}{\partial x^2}\right]_{\mathbf{r}=0} > 0 \quad \text{and} \quad \left[\frac{\partial^2 H_V(\mathbf{r})}{\partial y^2}\right]_{\mathbf{r}=0} > 0. \tag{8}$$

III. ANALYSIS AND NUMERICAL SIMULATIONS

A. Propagation and stability of gap vortex solitons

As seen from Fig. 1, the lowest domain of the existence of solitons is defined by $2\omega < \min\{\mathcal{E}^{(1)}_{1,-}, \mathcal{E}^{(2)}_{1,-}\}$. In this case, the solution belongs to the semi-infinite gaps of both components (this type of vortex solitons was reported in Ref. [17]). Other possibilities are determined by the existence of finite band gaps for the two components. It follows from the explicit forms of the operators introduced in Eq. (4) that, in the general situation, the SH spectrum has larger gaps than its FF counterpart; accordingly, at moderate values of ε_0, finite SH band gaps exist even if they are absent in the FF (this situation corresponds to the first vortex soliton considered in Ref. [17]). In Fig. 1 we show another situation, when the FF possesses one finite band gap in addition to the semi-infinite gap, while at least two finite band gaps are open in the SH.

This simple analysis of possible gap structures allows one to predict possible types of gap solitons. The expected soliton types may be classified by a pair of numbers (m,n) of the gaps in the FF and SH components, to which the soliton's frequencies belong. In other words, the localized modes belonging to total gap $\Delta_g^{(m,n)}$ are identified as (m,n) solitons ($\Delta_g^{(0,0)}$ will stand for the overlap of the semi-infinite gaps of both harmonics). Actually, we will concentrate on gap-vortex solitons (GVSs) of the (1,1) type, which belong to full band gap $\Delta_g^{(1,1)}$ shown in Fig. 1.

Typical examples of GVSs of the off-site and on-site types (alias square- and rhombus-shaped vortices, respectively [8]) are shown in Fig. 2. Unlike the 1D case, where localized modes can be constructed by means of the shooting method, allowing one to easily scan the entire gap and thus find the complete set of the solutions [21], in the 2D case it is necessary to resort to the relaxation method, using an initial guess with phase profiles $\exp(is\theta)$ carrying vorticities $s=1$ and $s=2$ in the FF and SH components, respectively. The intensity profiles in panels (a) and (b) feature sets of four peaks, for $2\omega=1$, which belongs to $\Delta_g^{(1,1)}$. The positions of the main peaks practically coincide with local minima (maxima) of the lattice potential for off-site (on-site) vortices. The phase distributions in panels (c) and (d) feature the phase shift of $\pi/2$ between adjacent peaks, as it should be in vortex patterns.

The application of Eq. (8) to the off- and on-site vortex families demonstrates that only the vortices of the former type (off-site alias "square" [8]) meet the necessary stability conditions. To perform the full stability inspection, we carried out direct simulations of Eqs. (1), using the split-step Fourier method and adding amplitude perturbations ~1% to the initial configurations in both FF and SH components. In Figs. 3(a) and 3(b), we show the intensity profiles as observed at $t=500$, which were generated by the perturbed off-site and on-site localized states shown in Fig. 2 (note that the characteristic diffraction distance for the patterns displayed in Fig. 2 is estimated as $t_{\text{diffr}} \sim 5$, hence $t=500$ corresponds to ~100 diffraction lengths, which is quite sufficient to make conclusions concerning the stability). The corresponding phase distributions are displayed in panels (c) and (d), respectively. It is concluded from Fig. 3 that the GVSs of the off-site (on-site) type are stable (unstable), in agreement with the prediction of Eq. (8). We have also tested a possibility to create asymmetric GVSs configurations with rectangular and

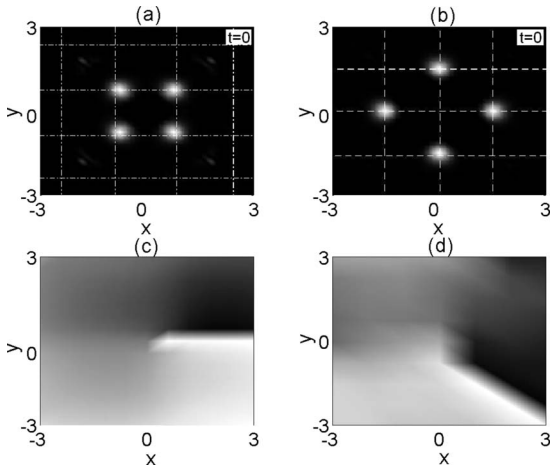

FIG. 2. Intensity profiles and phase distributions (upper and lower panels, respectively) of gap-vortex solitons for $2\omega=1$. Two examples of spatially localized solutions, (a) off-site and (b) on-site, are obtained from Eqs. (3) by means of the standard relaxation method for the same parameters as in Fig. 1. The dashed lines in (a) and (b) represent minima and maxima of the lattice potential, respectively.

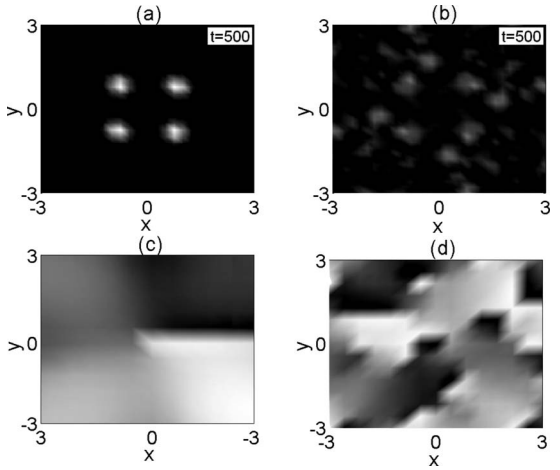

FIG. 3. Results of the evolution of the spatially localized solutions from Fig. 2, as produced by direct simulations of Eqs. (1), at $t=500$. The results are displayed only for the FF wave as for the SH component the situation is quite similar.

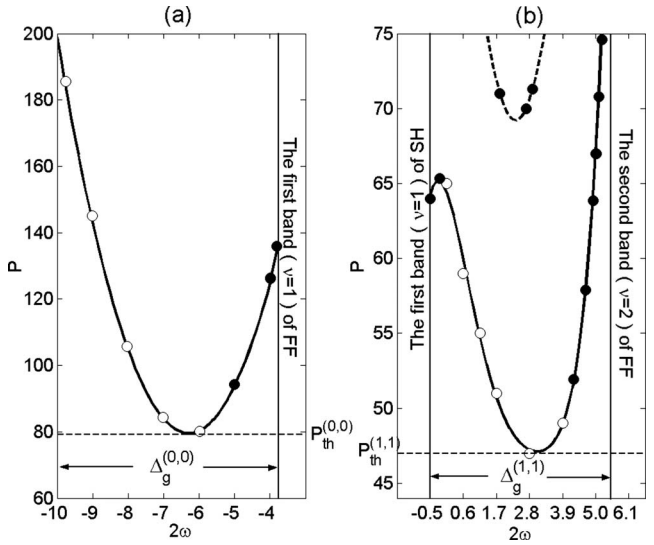

FIG. 4. (a) The lowest branch of the $P(\omega)$ curve for off-site GVSs of type (0,0) in the semi-infinite gap of the FF, $-\infty<2\omega<-3.7$. The minimum power necessary for the existence of these GVSs is $P_{\text{th}}^{(0,0)}\approx 80$, which is achieved at $2\omega\approx -6.3$. (b) The two lowest branches of $P(\omega)$ for GVSs of type (1,1) in the first lowest band, $-0.5<2\omega<5.5$. In the latter case, the power threshold is $P_{\text{th}}^{(1,1)}\approx 47$, achieved at $2\omega\approx 3.2$. In both panels, black and white circles correspond to unstable and stable solitons, respectively (the stability was tested by way of direct simulations).

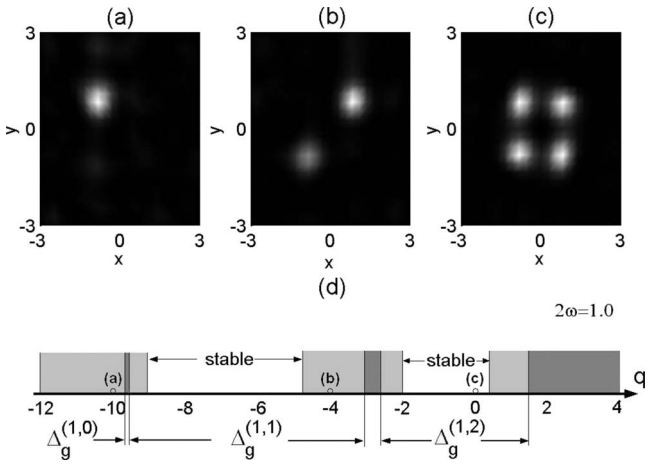

FIG. 5. The intensity profiles of the FF component of the off-site GVSs with $2\omega=1.0$ and phase mismatch (a) $q=-10$ (unstable), (b) $q=-4$ (unstable), and (c) $q=0$ (stable) after evolution time $t=500$. (d) Regions of the nonexistence (dark gray), instability (shadow gray), and stability (white) of the GVSs for a fixed frequency, $2\omega=1.0$, and different values of the phase mismatch, $-12<q<4$. The positions of the GVSs displayed in panels (a)–(c) are marked by the empty circles in (d).

triangular shapes, similar to those which were recently reported in lattices with the cubic nonlinearity [26]. However, we have found that both asymmetric configurations are unstable in the present model. This conclusion does not contradict the one obtained in the discrete model. Indeed, the band structure of the underlying linear continual model is essentially different, including an infinite number of bands (unlike the discrete model), hence unavoidable excitation of higher harmonics is likely a reason for the instability of the asymmetric vortices.

The dependence of total power carried by the GVSs of the off-site type on SH frequency 2ω (within the limits of the total gap) is shown in Fig. 4. We display two lowest branches of the (P,ω) curves in gap $\Delta_g^{(1,1)}$ and the lowest branch in $\Delta_g^{(0,0)}$. Note that there is a minimum (threshold) power required for the existence of $\chi^{(2)}$ solitons supported by the lattice potential in 2D [27], unlike the 1D case, where no such threshold exists [21]. Threshold power $P_{\text{th}}^{(1,1)}$ for the GVSs of the (1,1) type is lower than that for their counterparts of the (0,0) type, cf. panels (a) and (b) in Fig. 4. Note that the solitons located close to edges of the band gap are less stable than ones placed deeply inside of it. It is also worthy to note that the stability and instability of the solitons in this figure exactly comply with the Vakhitov-Kolokolov criterion, $dP/d\omega<0$ [28].

The existence and stability of the GVSs also depend on phase mismatch q when 2ω is fixed. Since q determines the position of the SH band-gap structure, we fix 2ω inside the FF gap and then vary q continuously. As long as 2ω stays outside of the SH gap, the GVSs cannot exist. If 2ω gets into the SH gap, the vortex solitons may be both stable and unstable. Their existence and stability regions are shown in Fig. 5.

B. Self-trapping of gap-vortex solitons

To explore the robustness of the GVSs, it is relevant to consider their self-trapping from Gaussian beams with embedded vorticity. To this end, we simulated the evolution of Gaussian pulses carrying the screw phase dislocation nested at its center,

$$\alpha_m(t=0)=A_m r^m e^{im\theta}e^{-r^2}[1+0.01\rho(x,y)], \quad m=1,2, \quad (9)$$

where $r=(x^2+y^2)^{1/2}$, A_m are amplitudes of the initial beam, and $\rho(x,y)$ is a broadband random function accounting for the initial perturbations. The simulations were performed in the presence and absence of the grating (periodic potential). If the grating is absent, the beams are broken by the azimuthal modulational instability into several fragments when the input power exceeds a certain threshold value, in accordance with the known scenario [4]. The fragments then move away along directions tangential to the initial ring, see Fig. 6(a). If the input power is taken below the splitting threshold, the ring-shaped beam spreads, decreasing its amplitude. If the grating is present, the vortical beams readily form stable GVSs, as shown in Fig. 6(b). This may happen at powers much lower than the splitting threshold in the free space.

Gaussian inputs [Eq. (9)] with different amplitudes A_m are able to generate GVSs belonging to different total gaps. In Fig. 6(b), we show the FF component of the vortex soliton with the same total power as that carried by the fragmented pattern in panel (a). The frequency of the soliton from panel (b) of Fig. 6 falls into $\Delta_g^{(0,0)}$, i.e., it is a vortex soliton of the (0,0)-type. In Fig. 6(c), we display the FF component of the GVS of the (1,1)-type, with the total power taken just above

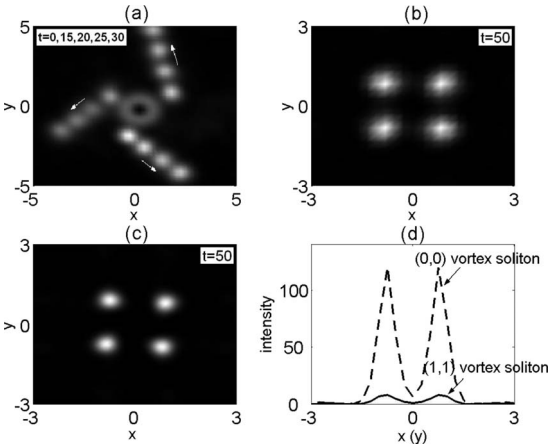

FIG. 6. The evolution of the input Gaussian pulse given by Eq. (9). (a) The initial vortex ring breaks along the azimuthal direction into three separating fragments. The panel is composed of intensity profiles obtained at different values of the propagation distance, *viz.*, $t=0$,15, 20, 25, and 30. The amplitudes of the initial beams are $A_1=A_2=14$, which corresponds to the total power just above the splitting power threshold. (b) The intensity profile of the FF component of the GVS, at $t=50$, with the same total power as in (a) but in the presence of the grating. In this case, $2\omega=-12.0$ belongs to semi-infinite gap $\Delta_g^{(0,0)}$ [the GVS of the (0,0) type], and $A_1=A_2=14$. (c) The intensity profile of the FF component of the GVS at $t=50$ in the presence of the grating. The total power is just above the threshold power necessary for the existence of GVSs. In this case, $2\omega=3.2$ belongs to $\Delta_g^{(1,1)}$ [the GVS of the (1,1) type] and $A_1=A_2=4.5$. (d) Comparison between the intensity profiles of the stable vortex solitons of the (0,0) and (1,1) types (dashed and solid lines, respectively).

the threshold necessary for the formation of the GVS of this type. It is worthy to note that the power of the (0,0) vortex soliton is usually higher than that of its (1,1) counterpart. Comparison between profiles of the vortex solitons of types (0,0) and (1,1), which are shown in panels 6(b) and (c), respectively, is presented in panel 6(d).

We have also studied the generation of GVSs from input beams containing solely the FF component. The respective results are shown in Fig. 7. The soliton is stabilized after rapid oscillations at the initial stage of the evolution, which account for the energy exchange between the FF and SH components. We can define the SH-generation efficiency, η, as the ratio of the total power in the SH component of the output to that of the input FF field, i.e.,

$$\eta(t)=\frac{P_2^{(\mathrm{out})}}{P_1^{(\mathrm{in})}}=\frac{\int|\alpha_2(t)|^2d\mathbf{r}}{\int|\alpha_1(t=0)|^2d\mathbf{r}}. \tag{10}$$

The efficiency may reach 15% for parameters used in Fig. 6 and still larger levels in other cases.

C. Delocalization transition of gap-vortex solitons

Threshold values of the total power needed for the generation of GVSs depend on the strength of the underlying

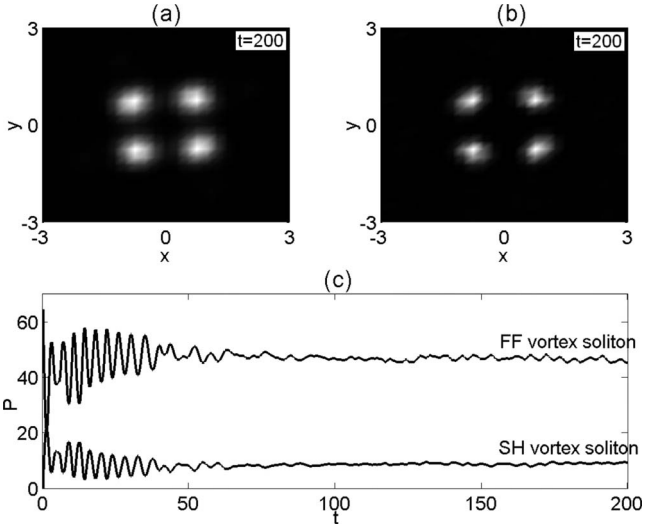

FIG. 7. The generation of the GVS from the FF input beam. The initial conditions are taken as per Eq. (9) with $A_1=9.0$ and $A_2=0$. The lattice parameters are the same as in Fig. 1. (a) The intensity profile of the FF component at $t=200$. (b) The intensity profile of the SH component at $t=200$. (c) The total powers of the FF and SH components (the upper and lower lines, respectively). The corresponding SH-generation efficiency is $\eta(t=200)\approx 0.15$.

grating, ε_0. In Fig. 8(a), we show the power threshold, in the form of $\ln(P_{\mathrm{th}})$ versus ε_0. Below the threshold, one can observe delocalization of vortex solitons. Actually, the GVSs of the (0,0)-type exist, in the semi-infinite gap, for any finite ε_0, while the GVSs of the (1,1)-type exist only for ε_0 exceeding some minimum (threshold) value, which is required to open the total gap $\Delta_g^{(1,1)}$ (i.e., the FF band gap $\Delta_1^{(1)}$, as the respective SH band gap already exists). In Fig. 8, P_{th} decreases with the increase in ε_0. In this connection, it is relevant to

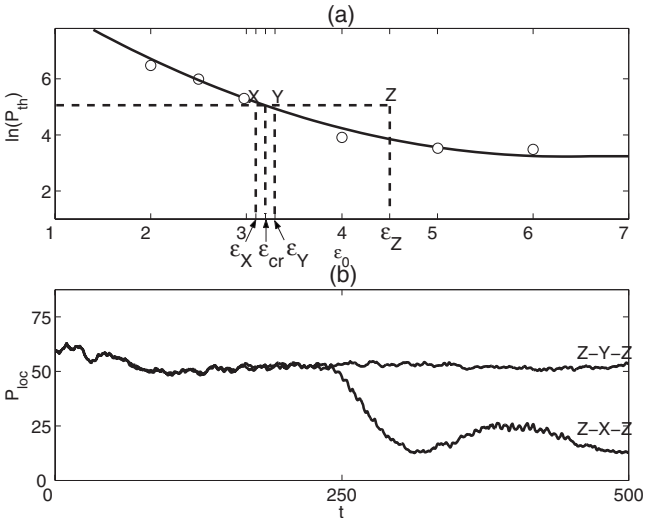

FIG. 8. (a) The existence border for GVSs, i.e., power threshold P_{th} versus the grating's strength ε_0, on the logarithmic scale. Along the existence curve, the solitons are stable, as shown by white circles. (b) The localized power, P_{loc}, versus t corresponding to adiabatic processes $Z\to Y\to Z$ and $Z\to X\to Z$. The parameters are $\varepsilon_Y=3.3$, $\varepsilon_X=3.1$, the respective critical value being $\varepsilon_{\mathrm{cr}}\approx 3.2$.

emphasize that stable GVSs cannot be supported either when the grating acts only on one of the components (i.e., when $\varepsilon_1\varepsilon_2=0$). Direct simulations (not shown here in detail) demonstrate that the beam decays in this case, via spreading out, the decay being slower when the grating is imposed on the FF (i.e., when $\varepsilon_1\neq 0$ and $\varepsilon_2=0$).

The existence of the power threshold is related to the phenomenon of the *delocalization transition*, which amounts to impossibility of restoring an initial localized state subject to an adiabatic change in the system's parameters when such change trespasses a properly defined border (see Ref. [24] for a brief review of the delocalization transitions). The lattice amplitude is a natural controlling parameter to govern such a transition, and a change in ε_0 may lead to dramatic consequences for the existence of GVSs.

To illustrate this phenomenon, we fix an initial lattice depth by designating $\varepsilon_0(t=0)\equiv\varepsilon_Z$. The respective initial conditions, indicated by point Z in Fig. 8(a), correspond to a GVS with total power $P\approx 60$. As the adiabatic variation in ε_0 conserves the total power, the change in ε_0 corresponds to a horizontal shift of the point in the plane of (ε,P), the dashed line in Fig. 8(a). To observe the delocalization transition, an initial decrease in ε_0 has to be followed by its increase back to the initial value, ε_Z. Denoting by $\varepsilon_{\rm cr}$ the intersection of the horizontal line with the existence border (the solid line) in Fig. 8(a), one can distinguish two possibilities. First, the decrease in ε_0 stops before reaching $\varepsilon_{\rm cr}$, say, at $\varepsilon_0=\varepsilon_Y>\varepsilon_{\rm cr}$. Second, ε_0 is decreased up to some value $\varepsilon_0=\varepsilon_X<\varepsilon_{\rm cr}$. These two possibilities correspond to routes $Z\to Y\to Z$ and $Z\to X\to Z$ in Fig. 8(a). In the former case the, GVSs exist along the entire route, hence one may expects that, at the end of the process, the initial soliton is (approximately) restored. In the latter case, however, a part of the route, which corresponds to $\varepsilon_X<\varepsilon<\varepsilon_{\rm cr}$, runs through the nonexistence region, where the soliton is destroyed and thus cannot be restored in the course of the further increase in ε_0.

These scenarios are indeed observed in numerical simulations, as shown in Fig. 8(b). To measure the power of the localized mode, we computed integral $P_{\rm loc}=\int_{-3}^{+3}(|\alpha_1|^2+2|\alpha_2|^2)d\mathbf{r}$, taken over a finite domain as a function of t (recall that the total power, computed over the entire integration domain, was preserved). For the of change in the lattice depth, we have set $\varepsilon_0(t)=\varepsilon_t+(\varepsilon_Z-\varepsilon\varepsilon_t)|1-2t/t_f|$, with $\varepsilon_t=\varepsilon_0(t_f/2)$. As one can see from the figure, for $\varepsilon_t>\varepsilon_{\rm cr}$ the solution indeed remains localized and recovers its initial profile at the end of the adiabatic change, while for $\varepsilon_t<\varepsilon_{\rm cr}$ the localized solution irreversibly spreads out.

IV. CONCLUSIONS

In this work, we have studied the existence and stability of 2D spatial GVSs (gap-vortex solitons) in the medium combining the quadratic nonlinearity and transverse grating, which is represented by the periodic modulation of the local refractive index. We have demonstrated that GVSs exist for frequencies belonging to one of the finite total gaps in the spectra of the FF and SH components. These vortex solitons of the gap type are different from solitary vortices previously found in the semi-infinite gap in Ref. [17]. The phase mismatch is an efficient tool for controlling the existence domains of the 2D solitons as one can change the number of the total gaps and their size by varying the mismatch. In addition to the analysis of the existence and stability of the GVS family in the first finite total gap, we have explored the self-trapping of the vortex solitons from input beams and the delocalization transition.

ACKNOWLEDGMENT

The work of C.H. was supported by the Fundação para a Ciência e a Tecnologia (FCT) under Grant No. SFRH/BPD/36385/2007.

[1] Y. S. Kivshar and G. P. Agrawal, *Optical Solitons: From Fibers to Photonic Crystals* (Academic, San Diego, 2003).

[2] R. Y. Chiao, E. Garmire, and C. H. Townes, Phys. Rev. Lett. **13**, 479 (1964).

[3] B. A. Malomed, D. Mihalache, F. Wise, and L. Torner, J. Opt. B: Quantum Semiclassical Opt. **7**, R53 (2005).

[4] W. J. Firth and D. V. Skryabin, Phys. Rev. Lett. **79**, 2450 (1997); D. V. Skryabin and W. J. Firth, Phys. Rev. E **58**, 3916 (1998).

[5] L. Torner and D. V. Petrov, Electron. Lett. **33**, 608 (1997); D. V. Petrov, L. Torner, J. Martorell, R. Vilaseca, J. P. Torres, and C. Cojocaru, Opt. Lett. **23**, 1444 (1998); J. P. Torres, J. M. Soto-Crespo, L. Torner, and D. V. Petrov, J. Opt. Soc. Am. B **15**, 625 (1998).

[6] M. Quiroga-Teixeiro and H. Michinel, J. Opt. Soc. Am. B **14**, 2004 (1997); A. Desyatnikov, A. Maimistov, and B. Malomed, Phys. Rev. E **61**, 3107 (2000); H. Michinel, J. Campo-Taboas, M. L. Quiroga-Teixeiro, J. R. Salgueiro, and R. Garcia-Fernandez, J. Opt. B: Quantum Semiclassical Opt. **3**, 314 (2001); B. A. Malomed, L.-C. Crasovan, and D. Mihalache, Physica D **161**, 187 (2002); D. Mihalache, D. Mazilu, L.-C. Crasovan, I. Towers, A. V. Buryak, B. A. Malomed, L. Torner, J. P. Torres, and F. Lederer, Phys. Rev. Lett. **88**, 073902 (2002); D. Mihalache, D. Mazilu, I. Towers, B. A. Malomed, and F. Lederer, J. Opt. A, Pure Appl. Opt. **4**, 615 (2002); H. Leblond, B. A. Malomed, and D. Mihalache, Phys. Rev. E **71**, 036608 (2005); A. S. Desyatnikov, D. Mihalache, D. Mazilu, B. A. Malomed, C. Denz, and F. Lederer, *ibid.* **71**, 026615 (2005); A. S. Desyatnikov, D. Mihalache, D. Mazilu, B. A. Malomed, and F. Lederer, Phys. Lett. A **364**, 231 (2007).

[7] B. A. Malomed and P. G. Kevrekidis, Phys. Rev. E **64**, 026601 (2001); B. B. Baizakov, B. A. Malomed, and M. Salerno, Europhys. Lett. **63**, 642 (2003); J. Yang and Z. H. Musslimani, Opt. Lett. **28**, 2094 (2003); B. B. Baizakov, B. A. Malomed, and M. Salerno, Phys. Rev. E **74**, 066615 (2006); T. Richter and F. Kaiser, Phys. Rev. A **76**, 033818 (2007); J. Wang and J.

Yang, *ibid.* **77**, 033834 (2008); R. Driben and B. A. Malomed, Eur. Phys. J. D **50**, 317 (2008).

[8] T. Mayteevarunyoo, B. A. Malomed, B. B. Baizakov, and M. Salerno, Physica D **238**, 1439 (2009).

[9] P. G. Kevrekidis, B. A. Malomed, Z. Chen, and D. J. Frantzeskakis, Phys. Rev. E **70**, 056612 (2004); H. Sakaguchi and B. A. Malomed, Europhys. Lett. **72**, 698 (2005); Phys. Rev. A **79**, 043606 (2009).

[10] D. N. Neshev, T. J. Alexander, E. A. Ostrovskaya, Yu. S. Kivshar, H. Martin, I. Makasyuk, and Z. Chen, Phys. Rev. Lett. **92**, 123903 (2004); J. W. Fleischer, G. Bartal, O. Cohen, O. Manela, M. Segev, J. Hudock, and D. N. Christodoulides, *ibid.* **92**, 123904 (2004); B. Terhalle, T. Richter, K. J. H. Law, D. Göries, P. Rose, T. J. Alexander, P. G. Kevrekidis, A. S. Desyatnikov, W. Królikowski, F. Kaiser, C. Denz, and Y. S. Kivshar, Phys. Rev. A **79**, 043821 (2009).

[11] A. Bezryadina, E. Eugenieva, and Z. Chen, Opt. Lett. **31**, 2456 (2006); D. Song, C. Lou, L. Tang, X. Wang, W. Li, X. Chen, K. J. H. Law, H. Susanto, P. G. Kevrekidis, J. Xu, and Z. Chen, Opt. Express **16**, 10110 (2008); H. Susanto, K. J. H. Law, P. G. Kevrekidis, L. Tang, C. Lou, X. Wang, and Z. Chen, Physica D **237**, 3123 (2008).

[12] B. Terhalle, T. Richter, A. S. Desyatnikov, D. N. Neshev, W. Królikowski, F. Kaiser, C. Denz, and Y. S. Kivshar, Phys. Rev. Lett. **101**, 013903 (2008).

[13] R. Driben, B. A. Malomed, A. Gubeskys, and J. Zyss, Phys. Rev. E **76**, 066604 (2007).

[14] A. Ferrando, M. Zacarés, and M. A. García-March, Phys. Rev. Lett. **95**, 043901 (2005).

[15] D. Mihalache, D. Mazilu, F. Lederer, B. A. Malomed, Y. V. Kartashov, L.-C. Crasovan, and L. Torner, Phys. Rev. Lett. **95**, 023902 (2005); H. Leblond, B. A. Malomed, and D. Mihalache, Phys. Rev. E **76**, 026604 (2007).

[16] D. Mihalache, D. Mazilu, L.-C. Crasovan, I. Towers, B. A. Malomed, A. V. Buryak, L. Torner, and F. Lederer, Phys. Rev. E **66**, 016613 (2002); D. Mihalache, D. Mazilu, B. A. Malomed, F. Lederer, L.-C. Crasovan, Y. V. Kartashov, and L. Torner, *ibid.* **74**, 047601 (2006).

[17] Z. Xu, Y. V. Kartashov, L.-C. Crasovan, D. Mihalache, and L. Torner, Phys. Rev. E **71**, 016616 (2005).

[18] Z. Xu and A. A. Sukhorukov, Opt. Lett. **34**, 1168 (2009).

[19] G. L. Alfimov, P. G. Kevrekidis, V. V. Konotop, and M. Salerno, Phys. Rev. E **66**, 046608 (2002).

[20] In particular, in the situations reported in Fig. 1 of Ref. [17], there indeed exist no vortex solitons below cut-off value b_{co} of the propagation constant (b), while in the case corresponding to Fig. 3 of the same work, we have found vortical modes in interval $1.0<b<2.7<b_{co}$.

[21] V. A. Brazhnyi, V. V. Konotop, S. Coulibaly, and M. Taki, Chaos **17**, 037111 (2007).

[22] A. Gubeskys, B. A. Malomed, and I. M. Merhasin, Phys. Rev. A **73**, 023607 (2006); S. K. Adhikari and B. A. Malomed, *ibid.* **77**, 023607 (2008).

[23] B. B. Baizakov and M. Salerno, Phys. Rev. A **69**, 013602 (2004).

[24] H. A. Cruz, V. A. Brazhnyi, V. V. Konotop, and M. Salerno, Physica D **238**, 1372 (2009).

[25] C. Etrich, F. Lederer, B. A. Malomed, T. Peschel, and U. Peschel, in *Progress in Optics*, edited by E. Wolf (North Holland, Amsterdam, 2000), Vol. 41, p. 483; A. V. Buryak, P. Di Trapani, D. V. Skryabin, and S. Trillo, Phys. Rep. **370**, 63 (2002).

[26] T. J. Alexander, A. A. Sukhorukov, and Y. S. Kivshar, Phys. Rev. Lett. **93**, 063901 (2004).

[27] M. I. Weinstein and B. Yearly, Phys. Lett. A **222**, 157 (1996); N. K. Efremidis, J. Hudock, D. N. Christodoulides, J. W. Fleischer, O. Cohen, and M. Segev, Phys. Rev. Lett. **91**, 213906 (2003).

[28] M. G. Vakhitov and A. A. Kolokolov, Izv. Vyssh. Uchebn. Zaved., Radiofiz. **16**, 1020 (1973) [Sov. J. Radiophys. Quantum Electron. **16**, 783 (1973)]; L. Bergé, Phys. Rep. **303**, 259 (1998).